

Topographic and crystallographic characterization of a grazing-ion-bombarded GaAs(110) surface by time-of-flight ion-scattering spectrometry

J. E. Gayone, R. G. Pregliasco, G. R. Gómez, E. A. Sánchez, and O. Grizzi

Centro Atómico Bariloche and Instituto Balseiro, Comisión Nacional de Energía Atómica and Consejo Nacional de Investigaciones Científicas y Técnicas, 8400 San Carlos de Bariloche, Río Negro, Argentina

(Received 3 December 1996; revised manuscript received 27 February 1997)

We studied the topography and the atomic structure of a clean GaAs(110) surface by time-of-flight ion-scattering spectrometry (TOF-ISS). In a first series of measurements the surface was cleaned by standard cycles of ion bombardment and annealing (500 eV Ar⁺, 500 °C). This method was very efficient to remove surface contaminants but not to smooth out the damage produced in TOF-ISS experiments. A cleaning method consisting of grazing bombardment with 20 keV Ar⁺ combined with annealing at 500 °C resulted in a clear improvement of the surface flatness. This was confirmed by measurements of electron energy distributions recorded under grazing proton bombardment and by a topographical analysis with an atomic force microscope. The crystallographic structure of the grazing ion bombarded surface was then studied by TOF-ISS. The quasisingle backscattered intensity measured for 5 keV Ne⁺ presented strong variations with the incident and azimuthal angles which are consistent with the generally accepted relaxed GaAs(110) surface. From the comparison of critical angles measured and focusing regions calculated with a code recently developed we have obtained an As-Ga first interlayer spacing $\Delta Z = (0.66 \pm 0.08) \text{ \AA}$, and the spacings between the first and second As layers $\Delta Z_{1,2}^{\text{As}} = (2.25 \pm 0.08) \text{ \AA}$ and between the first and second Ga layers $\Delta Z_{1,2}^{\text{Ga}} = (1.57 \pm 0.1) \text{ \AA}$. [S0163-1829(97)06728-3]

I. INTRODUCTION

Ion bombardment plays an important role in the cleaning, preparation, and characterization of semiconductor surfaces but, at the same time, it can create sufficient surface damage to change the electronic, growth, and adsorption properties of the surface. Several surface analysis techniques have been used to study the topography and the atomic structure of clean and adsorbate covered GaAs(110) surfaces. The technique of low-energy ion-scattering spectrometry (ISS) is sensitive to the surface elemental composition and topography, and provides valuable information about the surface atomic structure and adsorption sites. This is particularly important with H adlayers since most conventional techniques cannot detect H in direct ways. However, because of its inherently destructive nature and the high sensitivity of semiconductors to ion irradiation only in very few cases^{1,2} has it been used to study semiconductor surfaces, and to our knowledge it has never yet been applied to a GaAs(110) surface.

The damage produced in ISS can be strongly reduced by using time-of-flight techniques to analyze both ions plus neutrals in a multichannel method (TOF-ISS). In this case the bombarding dose required to acquire a spectrum amounts to $10^{11} - 10^{12}$ ions/cm², and typically between 5 and 20 spectra are taken as a function of the incident or azimuthal angle before a new annealing cycle is performed. The comparison of these fluences with those used in recent studies of damage produced on GaAs(110) surfaces³⁻⁵ indicates that the total doses used between annealings are well below that required for amorphization ($\sim 10^{15}$ ions/cm²). On the other hand, since each ion impact produces on average one multivacancy defect⁵ up to a small percentage of a monolayer can prove damaged between annealings. The successful applicability of the TOF-ISS technique will then depend on the capability to restore the surface order during annealing. In addition, in the

particular case of GaAs, if the annealing temperature is increased beyond 600 °C the surface starts to dissociate⁶ and droplets of metallic Ga are formed.

In the present work we apply TOF-ISS to study the topography and the atomic structure of a clean GaAs(110) surface. In the first part of the work we study the surface roughness resulting after performing several hours of TOF-ISS measurements on a surface cleaned with (a) repeated cycles of 500 eV Ar⁺ ion bombardment and annealing at 500 °C (IBA) and (b) grazing bombardment with 20 keV Ar⁺ and annealing at the same temperature. This last method has been successfully used before to prepare Al and Fe surfaces with large and atomically flat terraces.^{7,8} A qualitative characterization of the surface topography was obtained from (1) the backscattering intensity of neutrals plus ions measured in 5 keV Ne⁺ ion-surface collisions at low incident angles and (2) the electron emission produced at forward angles during 60 keV grazing H⁺ ion-surface collisions. After all the TOF-ISS measurements in the present work had been made, we checked the surface flatness with an atomic force microscope.

In the second part of this work we present a TOF-ISS study of the atomic structure of the GaAs(110) surface prepared by grazing-ion bombardment. The atomic structure of GaAs(110) surfaces, most of them prepared by cleavage, has been studied before by several surface analysis techniques, among them are low-energy electron diffraction^{9,10} (LEED), medium-energy ion scattering¹¹ (MEIS), and scanning tunneling microscopy¹² STM. It is known that the surface relaxes, preserving the 1×1 symmetry [Fig. 1(a)], and the plane of the surface chains rotates with respect to the surface plane, forming an angle $\omega \sim 25^\circ - 31^\circ$ [buckling angle, Fig. 1(b)]. The goal of this part of the work is to show that the surface prepared by grazing-ion bombardment also presents the relaxation of the cleaved surface and that TOF-ISS, com-

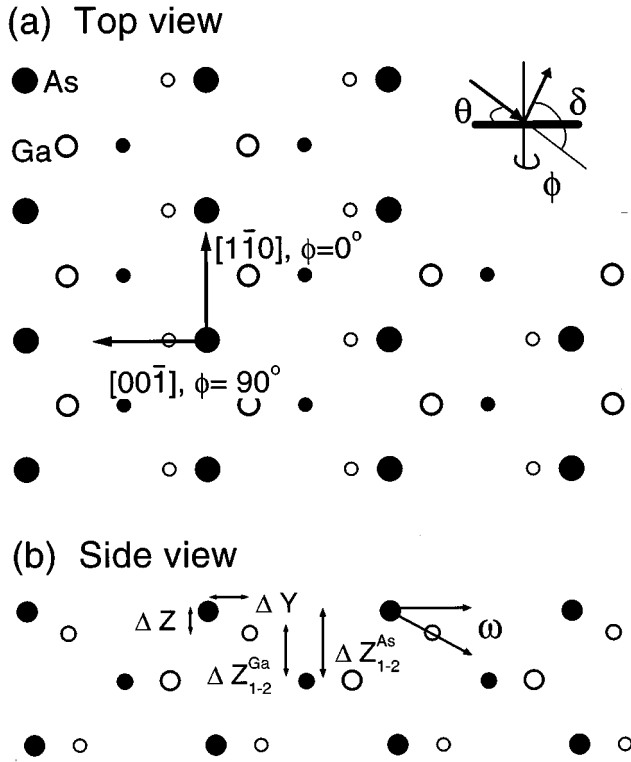


FIG. 1. (a) Top view of the GaAs(110) surface. The azimuthal angle is measured from the $[1\bar{1}0]$ direction. Inset: definition of the azimuthal (ϕ) and incident (θ) angles, the scattering angle δ is fixed at 107° . (b) Side view of the relaxed GaAs(110) surface. The buckling angle ω and characteristic interlayer spacings are indicated in the figure.

bined with grazing-ion bombardment and annealing, is very sensitive to this relaxation. The variations of the TOF spectra with the incident and azimuthal angles of the projectiles are interpreted in terms of shadowing and focusing effects calculated with a recently developed code. The results obtained in this part of the work will be used in a paper following this one where we study the adsorption of hydrogen on the GaAs(110) surface by TOF-ISS.

II. EXPERIMENTAL METHOD

Low-energy ISS and the techniques derived from it have been described in detail in several recent reviews.^{1,2,13} The information about the elemental composition is obtained from the energy analysis of keV ion projectiles scattered off the surface at large angles ($>90^\circ$) and from the recoiling target atoms they produce. For heavy targets the information about the surface atomic structure is derived from the dependence of the backscattered intensity with the incidence and azimuthal direction of the ions. Each target atom modifies the ion trajectories in a surface region of the order of 1 \AA^2 resulting in strong shadowing and focusing effects that are characteristic of the collision partners and of the surface geometry. Detection of both scattered ions plus neutrals by time-of-flight (TOF) methods avoids dealing with neutralization effects and reduces the ion bombardment dose required to obtain a spectrum by a factor of ~ 100 , therefore reducing the surface damage. The major disadvantage of the TOF

method is the appearance of a higher contribution from multiple-scattering sequences, making more uncertain the quantification of quasisingle scattering contributions.

The TOF-ISS measurements presented in this work were performed in a UHV chamber connected to a 4–100 keV ion accelerator which has been described previously.¹⁴ The chamber works at a base pressure of 6×10^{-10} Torr and has facilities for sputtering and Auger electron spectroscopy. The ions are generated in a radio frequency source, mass analyzed with a switching magnet and collimated to 0.1° of angular divergence. For TOF-ISS the ion beam is pulsed by two pairs of deflecting plates located at 40 cm from a slit whose width and height can be varied from 0 to 2.5 mm. Neutrals plus ions scattered at an angle of 107° are detected at the end of a 110.5 cm drift tube by a channeltron electron multiplier working with its cone grounded. All the TOF spectra shown in the present work were acquired at the same backscattering angle with a 5 keV $^{20}\text{Ne}^+$ ion pulsed beam of a 100 kHz rate and 80 nsec pulse width. We measured the pulse width and shape by collecting with the electron analyzer the electrons ejected during the beam-surface interaction and feeding this signal to the stop input of the time-to-amplitude converter.

The sample was a mirror-polished zinc-doped GaAs(110) disk of 8 mm diameter. It was mounted on a small goniometer custom-constructed with nonmagnetic materials which allows us to perform annealings up to 1500°C by electron bombardment from the back side of the sample. The ion incident angle (θ) can be varied from 0° to 107° with respect to the surface plane, and the azimuthal angle (ϕ) from -10° to 70° with respect to the main $[1\bar{1}0]$ surface channel [inset of Fig. 1(a)]. The crystallographic direction was determined *in situ* by monitoring surface channeling effects in specularly reflected 60 keV H^+ ions impinging at grazing incidence. The error in the incident and azimuthal angles was estimated in 0.25° and 0.5° , respectively.

The sample was cleaned by two different methods; at the beginning we used repeated cycles of 500 eV Ar^+ bombardment at 45° (15 min, $\sim 1 \times 10^{-8} \text{ A/mm}^2$), followed by 3 min annealing at 500°C . The temperature of the sample was measured with a thermocouple attached to the surface. After seeing that this method was not sufficient to improve the surface flatness we prepared the surface by cycles of 20 keV Ar^+ bombardment at incident angles between 1 and 2.5° (20 min, $1 \times 10^{-9} \text{ A/mm}^2$), followed by 3 min annealing at 500°C . During the Ar^+ bombardment the azimuthal orientation of the sample was continuously rotated.

III. SURFACE TOPOGRAPHY

In order to study the surface topography we measured TOF spectra along the $[1\bar{1}0]$ azimuthal direction as a function of the incident angle θ . At sufficiently small incident angles all the ions should be specularly scattered through a sequence of soft collisions and no backscattered projectiles should be detected at 107° , unless the surface has defects such as steps, adatoms, or vacancies which can enhance the probability of hard collisions.^{1,15,16} The inset of Fig. 2 shows a TOF spectrum acquired with 5 keV Ne^+ at $\theta = 18^\circ$. The narrow peaks correspond to quasisingle scattering (SS) off As and Ga surface atoms. Multiple scattering (MS) shows up

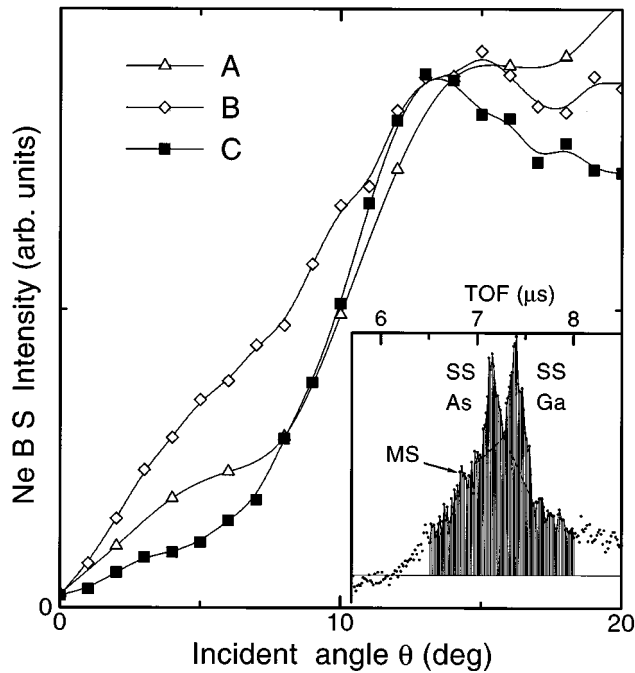


FIG. 2. Total (single plus multiple) Ne backscattering intensity measured along the $[1\bar{1}0]$ channel for the surface prepared by IBA (A,B) and by grazing Ar^+ bombardment (C). The inset shows a TOF spectrum measured along the $[1\bar{1}0]$ azimuth at $\theta=18^\circ$. The hatched area indicates the time window used to integrate the backscattering intensity shown in the figure.

as a broad contribution below the SS peaks. For these measurements, the total backscattering intensities (I_{tot}) were computed as the count integral over a region of $1.5\mu\text{sec}$ (hatched area). This time window is larger than the width corresponding to the SS peaks, and includes most of the MS contribution as well as the SS from both As and Ga atoms. Figure 2 shows Ne I_{tot} as a function of the incident angle for three different stages of the surface: (A) the surface prepared by IBA cycles with less than 2 h of TOF-ISS measurements (3.3×10^{13} ions/cm²), (B) after 6 h of TOF-ISS measurements (10^{14} ions/cm²) with intermediate IBA cycles, and (C) after treating the surface of (B) with ~ 50 cycles of grazing Ar^+ bombardment and annealing. The rise in I_{tot} at $\theta \sim 10^\circ$ is due mainly to the appearance of quasisingle backscattering off both As and Ga first and second atomic layers, which are similarly exposed to the beam along this incidence direction [Fig. 1(a)]. Although we cannot give a quantitative estimate of the surface flatness from these measurements, the continuous increase of Ne I_{tot} in curve B (surface prepared by IBA) corresponds to a surface with a large amount of surface defects.^{15,16} The sharper rise observed around $\theta=10^\circ$ for the same sample after applying the grazing-ion-bombardment treatment (curve C) clearly indicates an important improvement of the surface flatness. At larger incident angles, the contribution of the deeper layers to the backscattering intensity (not shown) remained almost the same for the three surfaces, indicating that the damage was produced mainly in the first two atomic layers.

The improvement in the surface flatness has also been tested by recording the forward electron emission produced during the bombardment of the sample with 60 keV H^+ ions

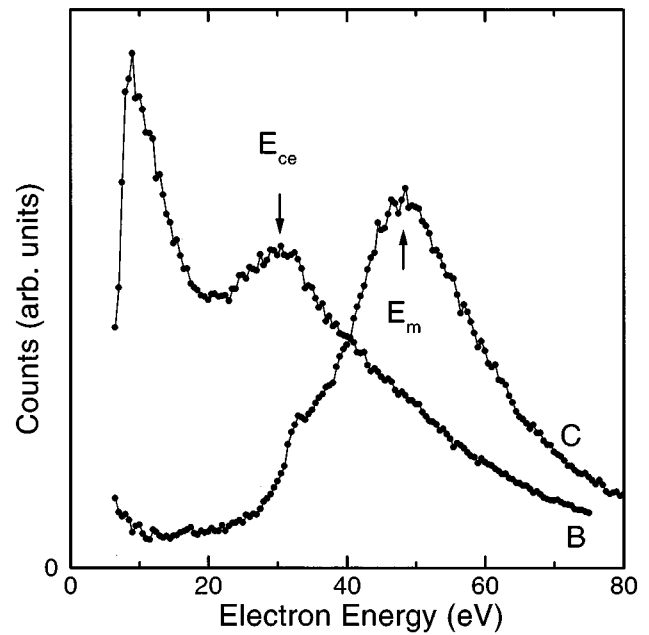


FIG. 3. Energy distribution of electrons ejected during 60 keV H^+ bombardment of the GaAs(110) surface prepared by IBA (B) and by grazing Ar^+ bombardment (C). The incident angle is 1° and the observation is made along the specular reflection of the ions.

at 1° of incidence. At this incidence condition, the ions travel approximately 100 \AA parallel to the surface before increasing the distance to the topmost atomic layer in 1 \AA . In this condition the probability of violent collisions with target atoms located at steps is large even for surfaces with a low density of impurities and defects. It was shown previously by Sánchez *et al.*^{18,19} that the energy distribution of the electrons ejected close to the direction of the ion specular reflection is very sensitive to the surface topography. Figure 3 shows the electron spectra corresponding to the surfaces characterized by curves B and C in Fig. 2. For the IBA-prepared surface, spectrum B in Fig. 3 shows strong emission at low energy (secondary electrons) and an intense peak at an energy E_{ce} that corresponds to electrons traveling with the same velocity as the projectiles (convoy electrons). This peak is determined by the electrons that recede from the target in close spatial correlation with the ion and interact with its Coulomb potential.²⁰ Both contributions (secondary and convoy electron peaks) reflect the strong ion-surface interaction and should decrease for smooth surfaces.¹⁸ In the case of the surface prepared by the grazing-bombardment method a new peak appears in the electron distribution at an energy E_m higher than E_{ce} (spectrum C in Fig. 3). This peak is observable only in surfaces with large and flat terraces¹⁸ and is ascribed to the interaction between the ejected electron and the ion- and electron-induced surface potentials.

The roughness detected after cleaning the surface with the IBA cycles indicates that for the GaAs(110) surface this method is not good enough to smooth out the surface damage produced during ion bombardment. Previous measurements^{3-5,17} have shown that GaAs surfaces are particularly sensitive to ion bombardment, and the present results indicate that even the small doses used in the TOF-ISS

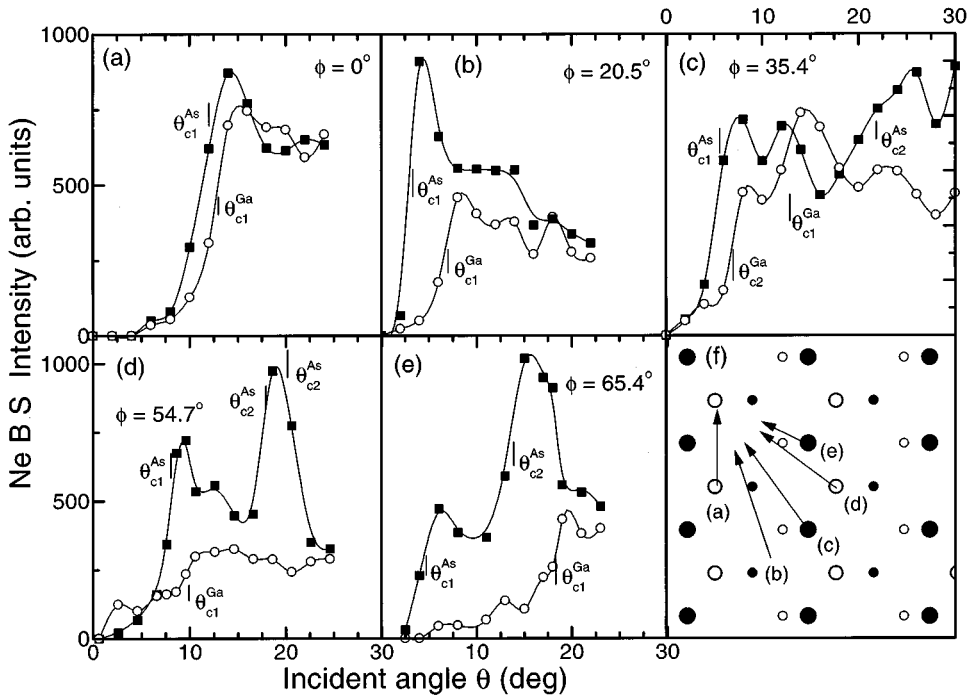


FIG. 4. $I_{BS}(\text{As})$ (solid squares) and $I_{BS}(\text{Ga})$ (open circles) vs θ measured for 5 keV Ne^+ along different azimuthal angles. The vertical segments indicate the position of the critical angles. (f) Top view of the GaAs(110) surface. The arrows indicate the azimuthal directions used to measure the incident scans.

measurements can produce an appreciable surface damage. On the other hand, preparation of the surface with repeated cycles of 20 keV Ar^+ grazing ion bombardment and annealing can produce a reasonably flat surface (Fig. 2, curve C) even starting from a relatively rough one (curve B). The improvement in the surface flatness is due to the fact that at grazing incidence the ions transfer a large amount of energy mainly to surface atoms located at steps; at flat terraces they scatter through a sequence of soft collisions without producing appreciable damage. This is why, before taking the TOF-ISS measurements discussed in the next section, the surface was prepared with the grazing-bombardment cycles during 4 h. After all the TOF measurements shown in this work had been made a characterization of the surface topography was performed by means of an atomic force microscope in air. The images show that for regions of $1\mu\text{m}^2$ the total variation in the height is smaller than 50 \AA , with large areas ($>1000\text{ \AA}$) where the height variations are just a few \AA .

IV. CRYSTALLOGRAPHIC STRUCTURE

The results presented above indicate an improvement of the surface flatness after applying the grazing Ar^+ bombard-

ment and annealing cycles; however, it is interesting to know if the surface also has a good crystallographic order. In the following section we present a TOF-ISS study of the atomic structure for the grazing-bombarded surface. The results and methodology described in this section will be used in the following paper to study the surface delaxation induced by hydrogen adsorption.

A. Incident and azimuthal scans

TOF spectra of neutrals plus ions were measured as a function of both the incident angle θ for several fixed azimuthal directions ϕ , and the azimuthal angle ϕ for fixed θ . The quasisingle backscattering intensities (I_{BS}) coming from As and Ga atoms (Figs. 4 and 5) were computed by integration of the corresponding SS peaks after a linear background subtraction (dashed line in the inset of Fig. 2). At certain incident and azimuthal angles the intensities present strong variations due to focusing of the ion trajectories on the target atoms. The critical angles, measured at 70% of the rise are indicated in the figures as vertical segments. For most directions, the critical incident angle necessary to focus the ions on As atoms are lower than those required for Ga atoms.

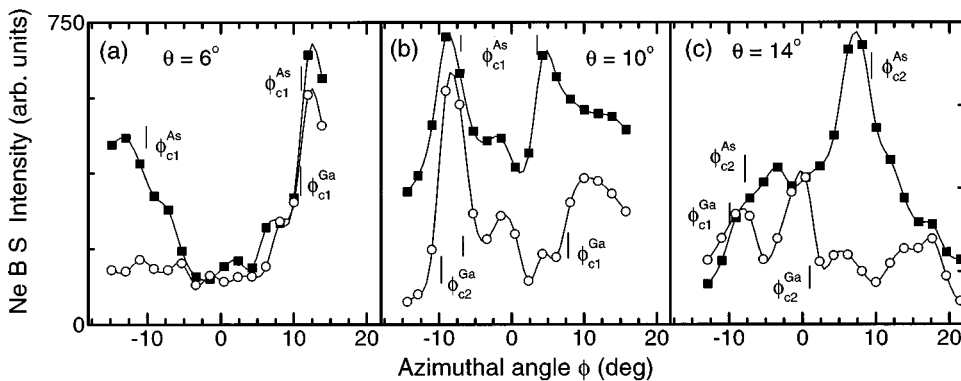


FIG. 5. Similar to Fig. 4, measured as a function of the azimuthal angle.

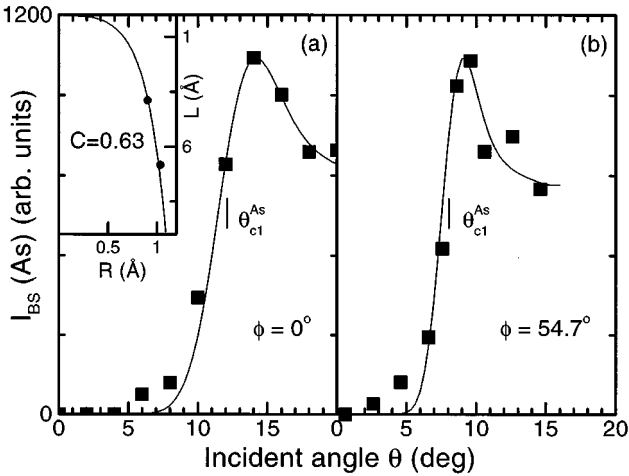


FIG. 6. Experimental and hitting probability calculation of $I_{BS}(As)$ vs θ for 5 keV Ne^+ along $\phi=0^\circ$ (a) and $\phi=54.7^\circ$ (b). The interatomic distances used for the calculation are those of the bulk, $d=4.00 \text{ \AA}$ and $d=6.92 \text{ \AA}$, respectively. The inset shows a shadow cone calculated with Oen's expression, and the solid symbols are the shadow cone dimensions obtained from the experimental critical angles.

This is consistent with a relaxed surface geometry where the first layer of Ga atoms (GaI) is deeper than that corresponding for As atoms (AsI). The azimuthal scans (Fig. 5) provide information about the symmetry of the surface and are a good complement to the incident scans. For example, at $\theta=6^\circ$ [Fig. 5(a)] $I_{BS}(As)$ is symmetric with respect to the $[1\bar{1}0]$ direction ($\phi=0^\circ$), while $I_{BS}(Ga)$ is strongly asymmetric. This difference can also be interpreted in terms of the relaxed surface geometry, i.e., at low incident angles only AsI and GaI contribute. AsI is higher and is not affected by shadowing from GaI; backscattering from AsI is thus symmetric with respect to the $[1\bar{1}0]$ channel. On the other hand, backscattering from GaI is strongly affected by shadowing from AsI. The second layer starts to contribute at larger incident angles and new focusings appear [Figs. 5(b) and (c)].

In order to identify the origin of the variations in the quasisingle backscattering intensity the experimental I_{BS} have to be compared with some sort of calculations. These can vary from a full trajectory simulation for the proposed atomic structure, as is obtained with the Marlowe code,²¹ to a simple calculation of the shadow cones produced by surface atoms. In this work we have used a recently developed code²² that calculates the shadowing regions for a particular layer, i.e., where backscattering towards the detector in a single collision is not possible due to shadowing by neighboring atoms. These calculations and the calibration of the interatomic potential are briefly described in the following section.

1. Calculation of shadowing diagrams

Following the ideas of Marchut *et al.*²³ and Overbury²⁴ the code displays the shadowing regions in the main parameters of the experiment, i.e., the projectile incident angle θ and the azimuthal direction ϕ . The code uses Oen's universal expressions for the shadow cone²⁵ and a mapping between shadowing and blocking whose details will be pub-

lished elsewhere.²² Oen's expressions are based on the Thomas-Fermi interatomic potential with the Molière approximation. In most calculations of shadow cones, the Firsov screening length is multiplied by a calibrating factor C . In our calculations C was obtained by fitting a calculated shadow cone (C being the fitting parameter) through two points obtained from measurements performed along azimuths with known interatomic distances. This is the case along the directions $\phi=0^\circ$ and $\phi=54.7^\circ$, where the low incidence rises in $I_{BS}(As)$ are the result of focusing from other As atoms placed at $d=4.00$ and 6.92 \AA , respectively. For the experimental points we used the shadow cone expressions $R=d\sin\theta_c+b$ and $L=d\cos\theta_c$, with b the impact parameter for scattering into 107° and θ_c the experimental critical angle. For reasons that will be discussed below, θ_{c1}^{As} was measured at 70% of the $I_{BS}(As)$ rise [Figs. 6(a) and (b)]. The inset of Fig. 6 shows the shadow cone calculated with $C=0.63$ (best fit), together with the experimental points. Along $\phi=35.4^\circ$ the $I_{BS}(As)$ rise at low θ is also caused by focusing between two As atoms with a known interatomic distance. However, since the Ne projectile passes close to a Ga atom, its trajectory is perturbed and the quasisingle model cannot be applied with confidence.

The calibrating screening factor for the Ne-Ga interatomic potential could be obtained in a similar way from $I_{BS}(Ga)$ measured along $\phi=0^\circ$. Along this azimuth the focusing on GaI atoms is produced by other GaI atoms placed at a distance that does not change with the surface relaxation. However, we will see later that along this direction there is a focusing from AsI onto Ga atoms of the second layer (GaII), that makes uncertain the calibration of C for the Ne-Ga collision. In the other azimuthal directions the focusings are produced by As atoms placed at interatomic distances that change with the relaxation; thus, they cannot be used to obtain C . For these reasons and considering that the As and Ga atoms have similar atomic numbers we have used the calibrating screening factor C obtained above for both Ne-As and Ne-Ga collisions.

For a perfectly flat surface, the sharpness of the rise in I_{BS} is determined by the vibration amplitude of the surface atoms, the interatomic distance, and the interatomic potential. If these parameters are known, the dependence of I_{BS} with θ can be calculated with the hitting probability method proposed by Daley *et al.*²⁶ We used this method to reproduce the experimental $I_{BS}(As)$ at $\phi=0^\circ$ and $\phi=54.7^\circ$, leaving C as a fitting parameter. Figures 6 (a) and (b) present the calculated $I_{BS}(As)$ using a vibration amplitude of 0.09 \AA taken from LEED experiments²⁷ and $C=0.63$, together with the experimental points. The good agreement between experimental and calculated data gives us confidence in the use of $C=0.63$. We have chosen to measure the critical angles at 70% of the I_{BS} rises because in this way, both methods used to calibrate the interatomic potential give the same screening calibration factor; although other positions ranging from 50 to 80% have been used by other researchers.^{1,2}

2. Comparison of experimental and calculated focusing directions

Since most adsorbates tend to remove the relaxation of the clean surface, it is worthwhile to knowing how sensitive

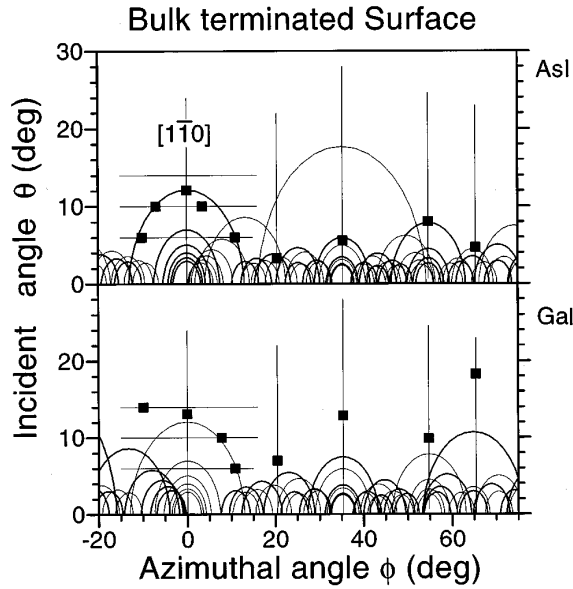


FIG. 7. Shadowing regions for a bulk terminated GaAs(110) surface calculated for 5 keV Ne^+ backscattering from the first (AsI) layer of As atoms (thick line) and first (GaI) layer of Ga atoms (thin line). The vertical and horizontal segments indicate the span of the incident and azimuthal scans, respectively; the solid symbols are the critical angles obtained from Figs. 4 and 5.

the technique is to this relaxation. We therefore start this section by briefly comparing the experimental critical angles with shadowing regions calculated for the bulk terminated surface. Figure 7 shows these regions for the first layers discriminated by type of atom (AsI, GaI). Each curve (or distorted circle) corresponds to the shadow region produced by a single atom, i.e., to incidence directions such that the beam cannot have small impact-parameter collisions with the atoms of the specified layer. For example, for AsI atoms the regions are produced by other AsI atoms (thick line) and also by GaI atoms (thin line). The edges of the shadow regions correspond to the focusing of the incident beam onto AsI atoms and should be compared directly with the measured

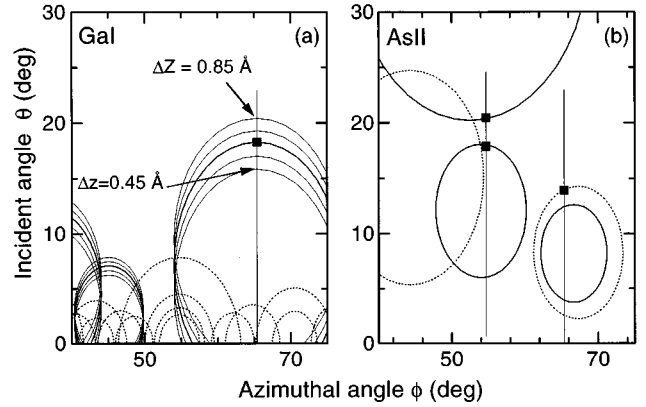


FIG. 8. (a) Shadowing regions for Ga atoms of the first layer due to other Ga atoms (dotted lines) and to As atoms (full lines) for different vertical spacings. The thick line corresponds to the vertical spacing that best fits the critical angle measured along $\phi = 65.4^\circ$. (b) Shadowing regions for As atoms of the second layer due to Ga atoms (dotted lines) and to other As atoms (full lines) that give the best fit to the measured critical angles.

critical angles (θ_c), which are also shown in Fig. 7 as solid symbols. The large disagreement observed for both AsI and GaI is due to the fact that for a bulk terminated surface AsI and GaI atoms are at the same height; in comparison with the relaxed surface where the shadowing should be stronger on AsI and weaker on GaI.

In order to determine the AsI-GaI interlayer spacing (ΔZ) we have calculated the GaI shadowing regions for ΔZ varying from 0.45 to 0.85 Å. The results of the calculation are shown in Fig. 8(a), together with the experimental critical angle measured for this region. We chose $\phi = 65.4^\circ$ because the interatomic distance involved in the focusing effect is short; thus a small change in ΔZ should produce a large change in the critical angle.²⁹ Along $\phi = 65.4^\circ$ the best agreement is obtained for $\Delta Z = (0.66 \pm 0.08)$ Å, equivalent to a buckling angle $\omega = (27 \pm 2)^\circ$. The latter was obtained by using the lateral displacement proposed in Ref. 10. Note that the difference in the critical angle calculated for interlayer

TABLE I. Comparison of the vertical spacing between AsI and GaI (ΔZ), the displacements of each layer measured from the bulk terminated surface (ΔZ^{Ga} and ΔZ^{As}), and the buckling angle ω obtained with different techniques.

ΔZ (Å)	ΔZ^{Ga} (Å)	ΔZ^{As} (Å)	ω (deg)	Technique
0.686	-0.527	0.159	31.1	LEED ^a
0.6858	-0.5099	0.1759	27.95	LEED ^b
0.708	-0.515	0.193	30.13	LEED ^c
0.7	-0.51	0.19	28.4	LEED ^d
0.71	-0.51	0.2	29 ± 3	MEIS ^e
			30	STM ^f
0.5	-0.36 ± 0.03	0.14 ± 0.02	22 ± 2	GIXD ^g
0.632	-0.348	0.284	26 ± 3	PD ^h
0.66 ± 0.08	-0.43 ± 0.1	0.25 ± 0.08	27 ± 2	TOF-ISS ⁱ

^aReference 9.

^bReference 10.

^cReference 30.

^dReference 31.

^eReference 11.

^fReference 12.

^gGrazing incidence x-ray diffraction (Ref. 32).

^hPhotoelectron diffraction (Ref. 33).

ⁱThis work.

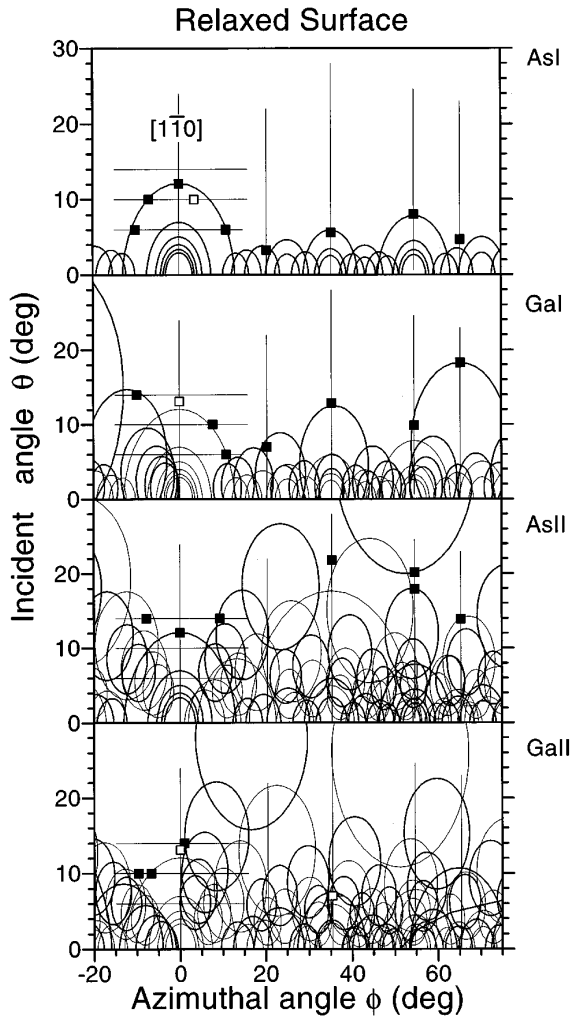


FIG. 9. Shadowing regions for the relaxed GaAs(110) surface calculated for 5 keV Ne^+ backscattering from the first (AsI), second (AsII) layer of As atoms (thick line), and first (GaI), second (GaII) layer of Ga atoms (thin line). The vertical and horizontal segments indicate the span of the incident and azimuthal scans, respectively; the solid symbols are the critical angles obtained from Figs. 4 and 5.

spacings differing in 0.1 \AA is $> 1^\circ$, which is somewhat bigger than the experimental error in the critical angle.

The focusings on AsII atoms can be used to determine the AsI-AsII and GaI-AsII interlayer spacings [$\Delta Z_{12}^{\text{Ga}}$ and $\Delta Z_{12}^{\text{As}}$ in Fig. 1(b)]. Along $\phi = 65.4^\circ$ there is focusing on AsII atoms produced by GaI atoms; the corresponding experimental critical angle is $\theta_{c2}^{\text{Ga}} = 13.9^\circ$, Fig. 4(e). On the other hand, along $\phi = 54.7^\circ$ there is a double focusing on AsII atoms due to two AsI atoms [Fig. 8(b)]. The corresponding critical angles are $\theta_{c2}^{\text{As}} = 17.9^\circ$ and $\theta_{c3}^{\text{As}} = 20.3^\circ$, Fig. 4(d). The best agreement between the edges of the shadowing regions and these critical angles is obtained for $\Delta Z_{1,2}^{\text{Ga}} = (1.57 \pm 0.1) \text{ \AA}$ and $\Delta Z_{1,2}^{\text{As}} = (2.25 \pm 0.08) \text{ \AA}$ [Fig. 8(b)]. Assuming that the position of the second layer atoms does not change with relaxation, AsI atoms move up by $\Delta Z^{\text{As}} = (0.25 \pm 0.08) \text{ \AA}$ and GaI atoms down by $\Delta Z^{\text{Ga}} = (-0.43 \pm 0.1) \text{ \AA}$. These values give a AsI-GaI spacing, $\Delta Z = \Delta Z^{\text{As}} - \Delta Z^{\text{Ga}} = (0.68 \pm 0.18) \text{ \AA}$, which is very similar to that obtained

above and is in excellent agreement with those obtained by other techniques (Table I).

With the vertical displacements obtained above and the lateral displacements given by Tong *et al.*¹⁰ we have calculated the new shadowing regions for AsI, GaI, AsII, and GaII, and compared them with all the experimental critical angles in Fig. 9. With the exception of very few points (some of which will be discussed below) the experimental data are all located at the edges of the shadowing regions. The agreement is very good even for those focusings where the pair of participating atoms is not aligned with the projectile direction. The shadowing regions of Fig. 9 allow us to identify easily the origin of the focusing directions; we can assign them to a specific layer and identify the pair of atoms involved in the focusing effect. The good agreement with this simple calculation also indicates that most of the focusings seen at low θ in the relatively open GaAs(110) surface can be well described in a two-atom picture. There are, however, directions where this model fails to reproduce the observed focusing effect (see open squares in Fig. 9). For example, along $\phi = 35.4^\circ$ the contribution from GaII appears at a small incident angle and seems to be due to a multiple scattering sequence [Fig. 4(c), θ_{c2}^{Ga}]. Another case can be observed for GaI along $\phi = 0^\circ$ where, as we can see from the GaII shadowing regions, the focusing on GaII atoms is affected by a row of AsI atoms (Fig. 9). This contribution from GaII cannot be separated from that coming from GaI; we believe this is the reason for the disagreement between measured and calculated GaI critical angles. A similar effect on AsII might be responsible for the disagreement observed in AsI along the azimuthal scan taken at $\theta = 10^\circ$. A trajectory calculation including multiple collisions is necessary to describe these focusing effects.

V. SUMMARY AND CONCLUSIONS

In the first part of the work we studied the GaAs(110) surface topography resulting from TOF-ISS measurements and two preparation methods: standard IBA cycles and grazing-ion bombardment and annealing cycles. Experiments of TOF-ISS performed at low incident angles and of electron emission in grazing H^+ -surface collisions confirm the high sensitivity to ion irradiation of the GaAs(110) surface. Even at the low fluences used in the TOF-ISS measurements the surface deteriorates (mainly the first atomic layer) and the IBA cycles are not sufficient to restore its initial flatness and order. On the other hand, cycles of grazing bombardment with 20 keV Ar^+ ions and annealing at the same temperature used in IBA, produce a clear improvement in the surface flatness, and allowed us to perform prolonged TOF-ISS measurements without appreciable damage.

In the second part of the work we studied the atomic structure of the grazing bombarded GaAs(110) surface by TOF-ISS. The TOF resolution was good enough to separate the As and Ga quasisingle scattering contributions; thus enabling us to identify the backscattering off first and second layers. The dependence of the Ne backscattering intensity with incident and azimuthal angles is consistent with the generally accepted surface relaxation. The experimental critical angles obtained for processes coming from both first and second atomic layers were compared with a calculation of

shadowing regions. This comparison allowed us to identify the atoms involved in the focusing effects. The best agreement between the critical angles and the edges of the shadowing regions was obtained for an AsI-GaI interlayer spacing $\Delta Z = (0.66 \pm 0.08) \text{ \AA}$. From particular directions we obtained distances from As and Ga first layers to the second layer $\Delta Z_{1,2}^{\text{Ga}} = (1.57 \pm 0.1) \text{ \AA}$ and $\Delta Z_{1,2}^{\text{As}} = (2.25 \pm 0.08) \text{ \AA}$, which are in excellent agreement with those obtained by other techniques. The crystallographic results and the methodology to obtain them from TOF-ISS measurements will be

used in the following paper to study the hydrogen covered GaAs(110) surface.²⁸

ACKNOWLEDGMENTS

We acknowledge very stimulating discussions with Lic. M. Passeggi, Jr. and Dr. J. Ferrón. This work was partially supported by CONICET (3292/92), Fundación Balseiro, Fundación Antorchas (A-12924/1), and Cooperativa de Electricidad Bariloche.

- ¹H. Niehus, W. Heiland, and E. Taglauer, *Surf. Sci. Rep.* **17**, 213 (1993).
- ²J. W. Rabalais, *Surf. Sci.* **299/300**, 219 (1994).
- ³H. Gnaser, B. Heinz, and H. Oechsner, *Phys. Rev. B* **52**, 14 086 (1995).
- ⁴R. J. Pechman, X.-S. Wang, and J. H. Weaver, *Phys. Rev. B* **51**, 10 929 (1995).
- ⁵B. D. Weaver, D. R. Frankl, R. Blumenthal and N. Winograd, *Surf. Sci.* **222**, 464 (1989).
- ⁶F. Proix, A. Akremi, and Z. T. Zhong, *J. Phys. C* **16**, 5449 (1983).
- ⁷A. G. Borisov, H. Winter, G. Dierkes, and R. Zimmy, *Europhys. Lett.* **33**, 229 (1996).
- ⁸H. Winter and J. Leuker, *Nucl. Instrum. Methods Phys. Res. B* **72**, 1 (1992).
- ⁹C. B. Duke, S. L. Richardson, A. Paton, and A. Kahn, *Surf. Sci.* **127**, L135 (1983).
- ¹⁰S. Y. Tong, W. N. Mei, and G. Xu, *J. Vac. Sci. Technol. B* **2**, 393 (1984).
- ¹¹L. Smit, T. E. Derry, and J. F. Van Der Veen, *Surf. Sci.* **150**, 245 (1985).
- ¹²R. M. Feenstra, J. A. Stroscio, J. Tersoff, and A. P. Fein, *Phys. Rev. Lett.* **58**, 1192 (1987).
- ¹³Th. Fauster, *Vacuum* **38**, 129 (1988).
- ¹⁴L. De Ferraris, F. Tutzauer, E. A. Sánchez and R. A. Baragiola, *Nucl. Instrum. Methods Phys. Res. A* **281**, 43 (1989).
- ¹⁵H. Niehus, *Surf. Sci.* **145**, 407 (1984).
- ¹⁶O. Grizzi, M. Shi, H. Bu, and J.W. Rabalais, *Chemistry and Physics of Solid Surfaces VII*, edited by Vanselov and Howe (Springer-Verlag Berlin, 1990), Chap 10.
- ¹⁷D. G. Welkie and M. G. Lagally, *J. Vac. Sci. Technol.* **16**, 784 (1979).
- ¹⁸E. A. Sánchez, O. Grizzi, M. L. Martiarena, and V. H. Ponce, *Phys. Rev. Lett.* **71**, 801 (1993).
- ¹⁹E. A. Sánchez, O. Grizzi, M. L. Martiarena, and V. H. Ponce, *J. Phys., Condens. Matter.* **5**, A289 (1993).
- ²⁰P. Focke, W. Meckbach, C. R. Garibotti, and I. B. Nemirovsky, *Phys. Rev. A* **28**, 706 (1983).
- ²¹M. T. Robinson and I. M. Torrens, *Phys. Rev. B* **9**, 5008 (1974).
- ²²R. G. Pregliasco, J. E. Gayone, E. A. Sánchez, and O. Grizzi (unpublished).
- ²³L. Marchut, T. M. Buck, G. H. Wheatley, and C. J. McMahon, Jr. *Surf. Sci.* **141**, 549 (1984).
- ²⁴S. H. Overbury, *Nucl. Instrum. Methods Phys. Res. B* **27**, 65 (1987).
- ²⁵O. S. Oen, *Surf. Sci.* **131**, L470 (1983).
- ²⁶R. S. Daley, J. H. Huang, and R. S. Williams, *Surf. Sci.* **215**, 281 (1989).
- ²⁷H.-J. Gossmann and W. M. Gibson, *J. Vac. Sci. Technol.* **2**, 343 (1984).
- ²⁸J.E. Gayone, R.G. Pregliasco, E.A. Sánchez, and O. Grizzi, *Phys. Rev. B* **56**, 4194 (1997).
- ²⁹For the bulk terminated surface the Ga and As atoms should be aligned along $\phi = 64.7^\circ$, instead of $\phi = 65.4^\circ$. The small difference is due to the change in ΔY [Fig. 1(a)] for the relaxed surface, which according to Tong *et al.* (Ref. 10) is around 0.1 Å. Since our sensitivity to lateral displacements is small, we decided to use the published value for the relaxed surface (Ref. 10).
- ³⁰M. W. Puga, G. Xu, and S. Y. Tong, *Surf. Sci.* **164**, L789 (1984).
- ³¹W. K. Ford, T. Guo, D. L. Lessor, and C. B. Duke, *Phys. Rev. B* **42**, 8952 (1990).
- ³²A. Ruocco, S. Nannarone, M. Sauvage-Simkin, N. Jedrecy, R. Pinchaux, and A. Waldhauer, *Surf. Sci.* **307-309**, 662 (1994).
- ³³A. Ruocco, M. Biagini, A. di Bona, N. Gambacorti, S. Valeri, and S. Nannarone, *Phys. Rev. B* **51**, 2399 (1995).